

Direct and Indirect Interlayer Excitons in a van der Waals Heterostructure of hBN/WS₂/MoS₂/hBN

Mitsuhiro Okada,^{†,¶} Alex Kutana,^{‡,¶} Yusuke Kureishi,[†] Yu Kobayashi,[§] Yuika Saito,^{||} Tetsuki Saito,[§] Kenji Watanabe,[⊥] Takashi Taniguchi,[⊥] Sunny Gupta,[‡] Yasumitsu Miyata,[§] Boris I. Yakobson,[‡] Hisanori Shinohara,^{*,†,¶} and Ryo Kitaura^{*,†,¶}

[†]Department of Chemistry, Nagoya University, Nagoya 464-8602, Japan

[‡]Department of Materials Science and NanoEngineering, Rice University, Houston, Texas 77005, United States

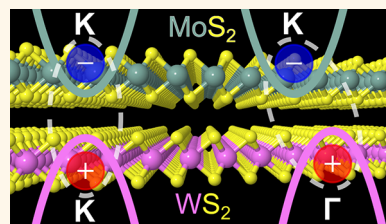
[§]Department of Physics, Tokyo Metropolitan University, Hachioji, Tokyo 192-0397, Japan

^{||}Department of Chemistry, Gakushuin University, Tokyo 171-0031, Japan

[⊥]National Institute for Materials Science, 1-1 Namiki, Tsukuba 305-0044, Japan

Supporting Information

ABSTRACT: A van der Waals (vdW) heterostructure composed of multivalley systems can show excitonic optical responses from interlayer excitons that originate from several valleys in the electronic structure. In this work, we studied photoluminescence (PL) from a vdW heterostructure, WS₂/MoS₂, deposited on hexagonal boron nitride (hBN) flakes. PL spectra from the fabricated heterostructures observed at room temperature show PL peaks at 1.3–1.7 eV, which are absent in the PL spectra of WS₂ or MoS₂ monolayers alone. The low-energy PL peaks we observed can be decomposed into three distinct peaks. Through detailed PL measurements and theoretical analysis, including PL imaging, time-resolved PL measurements, and calculation of dielectric function $\epsilon(\omega)$ by solving the Bethe–Salpeter equation with G_0W_0 , we concluded that the three PL peaks originate from direct K–K interlayer excitons, indirect Q– Γ interlayer excitons, and indirect K– Γ interlayer excitons.



KEYWORDS: transition metal dichalcogenides, van der Waals heterostructures, interlayer exciton, photoluminescence spectroscopy, density functional theory

Two-dimensional (2D) van der Waals (vdW) heterostructures, particularly those based on transition metal dichalcogenides (TMDs), offer opportunities to explore electronic and optical properties at the two-dimensional limit.^{1–5} TMDs possess layered structures in which a transition metal layer is sandwiched by chalcogen layers with trigonal prismatic or octahedral geometries.^{6–10} These layers are stacked to form bulk crystals of TMDs. Importantly, TMDs can be isolated in monolayer form owing to the weak interlayer vdW force.^{1,7,9} Recent studies have shown that monolayer TMDs, three-atom-thick atomic layers, can be assembled into vdW heterostructures with desired sequences.^{11–14} Although further development of fabrication methods is still necessary to achieve vdW heterostructures with fully controllable stacking sequences, these results suggest the exciting possibility of designing heterostructure 2D systems with customizable electronic band structures and physical properties.

The emergence of interlayer excitons in type-II vdW heterostructures of TMDs provides an opportunity to explore the basic physics of 2D excitons and valley degree of freedom

(VDOF).^{2,3,15} Monolayer TMDs in the 2H phase have hexagonal honeycomb frameworks, where A- and B-sites are occupied by transition metal and chalcogen atoms, respectively.^{10,16} 2H-TMDs possess two inequivalent valleys in their electronic bands at the corners of their hexagonal Brillouin zones (K and K' points), and the inequivalent K and K' points are the source of the VDOF.^{8,17} In monolayer semiconductor TMDs, such as WS₂ and MoS₂, the K and K' points correspond to direct energy gaps.¹⁸ Due to the enhanced many-body effect in 2D systems, strong excitonic transitions can be observed even at room temperature. Furthermore, in TMDs with an odd number of TMD layers, excitation by circular-polarized light can create photoexcited carriers selectively at K or K' points, thus yielding valley-polarized 2D excitons.^{17,19,20} These fascinating properties of TMDs can also be observed in vdW heterostructures composed of TMDs.^{2,3} Recent works on TMD

Received: November 21, 2017

Accepted: February 26, 2018

Published: February 26, 2018

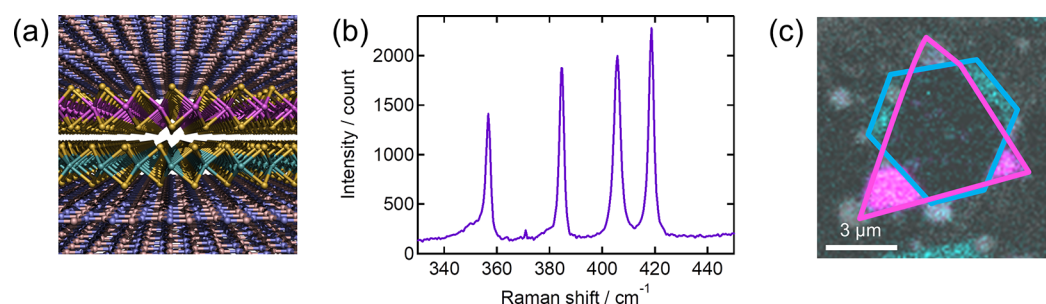


Figure 1. (a) Structural model of hBN/WS₂/MoS₂/hBN. Magenta, cyan, yellow, blue, and pink spheres represent tungsten, molybdenum, sulfur, nitrogen, and boron atoms, respectively. (b) Typical Raman spectrum from hBN/WS₂/MoS₂/hBN. (c) PL image of hBN/WS₂/MoS₂/hBN. This image combines transmission bright-field image (monochrome), 1.97–2.07 eV (magenta), and 1.71–1.91 eV detection (cyan). Magenta and cyan lines show the edge of WS₂ and MoS₂ crystals, respectively. To measure both the Raman spectrum and PL image, an excitation energy of 2.54 eV was used.

vdW heterostructures with type-II band alignment have shown that interlayer excitons, which have electrons and holes located in different layers, can be formed in such systems.^{1,12,21,22} Compared with intralayer excitons,^{20,23,24} interlayer excitons can have very long lifetimes (~ 138 ns) and valley depolarization lifetimes (~ 39 ns).^{2,22} Therefore, TMD vdW heterostructures with type-II band alignment provide an excellent platform to explore exotic 2D many-body excitonic states and introduce the potential of realizing valleytronic devices.

Exploration of basic exciton physics and the possibility for optoelectronic applications of a TMD-based type-II vdW heterostructure requires deeper understanding of the interlayer excitons that emerge in this system. TMDs are multivalley semiconductors in which intra- and intervalley excitons (electrons and holes located at the same or different valleys) can be formed by optical excitation.^{17,20} When used in heterostructures, interlayer interactions can cause changes in electronic bands accompanied by shifts in the energies of the valence band maximum (VBM) and the conduction band minimum (CBM). Under this condition, other valleys, including Γ and Q valleys, can contribute to optical transitions along with the contributions from K and K'.^{21,25,26} Furthermore, TMD-based heterostructures with different stacking angles can have different electronic band structures, where the CBM and VBM are located at different positions.²⁶ Therefore, various kinds of interlayer excitons can appear in TMD-based heterostructures, and these interlayer excitons can cause a range of optical responses.^{21,27,28} For example, direct and indirect interlayer excitons can form in TMD-based heterostructures through Coulomb interaction between electrons and holes located at various valleys. Direct and indirect interlayer excitons should show different exciton lifetimes and can carry VDOF differently, providing a range of optical responses in heterostructures. Photoluminescence (PL) peaks in a WS₂/MoS₂ heterostructure have been reported to originate from interlayer excitons corresponding to K–K and K– Γ transitions;²⁹ however, further spectroscopic characterization and theoretical analysis are necessary to fully elucidate the origin of these PL emissions.

Here, we report observations of three different interlayer excitons in PL spectra of a WS₂/MoS₂ heterostructure with type-II band alignment.^{25,30} We use hexagonal boron nitride (hBN) flakes as a substrate and apply an overlayer to form an hBN-encapsulated WS₂/MoS₂ sample (*i.e.*, hBN/WS₂/MoS₂/hBN) to observe fine structures in the heterostructure's optical

spectra. hBN is a layered insulator without dangling bonds on the surface, and hBN can protect WS₂/MoS₂ from substrate effects such as the inhomogeneous broadening in the optical transitions that are caused by surface roughness.^{31,32} In addition, we have, importantly, controlled the stacking angle in WS₂/MoS₂. As mentioned above, the electronic band structure of WS₂/MoS₂ depends on the stacking angle. Therefore, controlling the stacking angle is necessary to ascertain the origin of interlayer excitons. In previous studies, second-harmonic generation microscopy, which requires an ultrashort pulsed light source, was used for preparing the stacking-angle-controlled samples.² In this work, we report the development of a simple alternative dry-transfer-stamping technique with TMD crystals grown by chemical vapor deposition (CVD). The CVD-grown crystals typically have faceted zigzag edges,^{33,34} which indicate the crystal orientation during the transfer process, and we can easily and unambiguously control relative orientation between WS₂ and MoS₂ in a heterostructure. In a typical PL spectrum of hBN/WS₂/MoS₂/hBN with a stacking angle of $\sim 60^\circ$, we have observed three contributions in the energy region of 1.3–1.7 eV at room temperature. By comparing photoluminescence excitation (PLE) measurements and theoretical calculations, we have concluded that the three contributions originate from the following: (1) direct K–K interlayer excitons, (2) indirect Q– Γ interlayer excitons, and (3) K– Γ interlayer excitons. These findings provide a basis for further understanding the optical physics of TMD-based heterostructures.

RESULTS AND DISCUSSION

The heterostructure samples studied (hBN/WS₂/MoS₂/hBN) are prepared following the dry-transfer method with CVD-grown TMDs. First, we prepared WS₂/sapphire and MoS₂/hBN monolayers by CVD with a multifurnace CVD setup. Elemental sulfur is used as the sulfur source in both cases, and tungsten that was sputtered on sapphire and MoO₃ are used as the metal source while growing the WS₂/sapphire and MoS₂/hBN layers, respectively. The monolayer structure of the grown WS₂ and MoS₂ sheets was confirmed with an optical microscope and PL spectroscopy, respectively (Figure S1). Both contrast in optical images and PL peaks of monolayers are distinctly different from those of multilayers, leading to easy and sure confirmation of the monolayer structure. The crystal of monolayer WS₂ grown on a sapphire substrate was subsequently transferred to an hBN flake mounted on a poly(methyl methacrylate) (PMMA)/polydimethylsiloxane

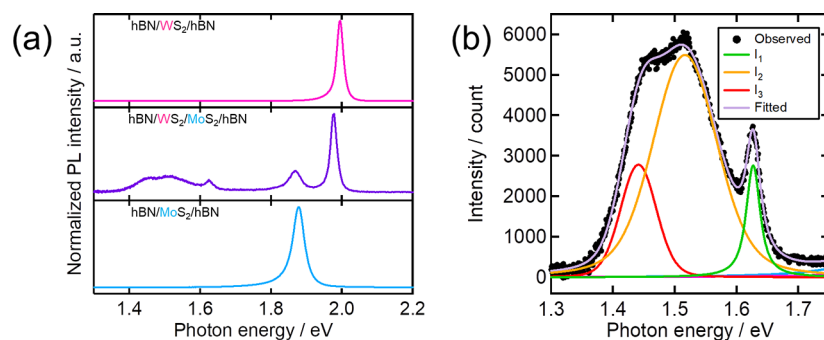


Figure 2. (a) PL spectra of hBN/WS₂/hBN, hBN/WS₂/MoS₂/hBN, and hBN/MoS₂/hBN measured at room temperature. An excitation energy of 2.54 eV was used to measure all spectra. (b) PL spectrum of hBN/WS₂/MoS₂/hBN at lower energy side with excitation energy of 2.33 eV. Contributions from I₁, I₂, and I₃, which are plotted with green, orange, and red curves, respectively, are modeled by a Voigt function.

(PDMS) film, after which the WS₂ on the hBN/PMMA/PDMS was placed onto a MoS₂/hBN crystal to form the hBN-encapsulated heterostructure, hBN/WS₂/MoS₂/hBN. After the transfer process, samples were heated at 200 °C for more than 10 h to ensure good physical contact between WS₂ and MoS₂. The postheating process has been proven to be important to make good physical contact between layers in a van der Waals heterostructure.³⁵ Figure 1a–c shows a schematic of hBN/WS₂/MoS₂/hBN, a typical Raman spectrum, and a typical PL image. The Raman spectrum of a hBN/WS₂/MoS₂/hBN with a 60° stacking angle (Figure 1b) shows four peaks at 356.7, 384.6, 405.7, and 418.6 cm⁻¹, which are consistent with the peaks observed in the Raman scattering from the E' and A' modes of monolayer MoS₂ and WS₂.^{12–14} As seen in the PL image (Figure 1c), PL is strongly quenched at the stacked region, which indicates that interlayer charge transfer is occurring efficiently across the interface between the layers.^{14,36}

This clean interface was also confirmed with low-frequency Raman spectroscopy. In a low-frequency Raman spectrum (Figure S2), the shear and breathing interlayer vibrational modes are clearly seen at 23.7 and 35.5 cm⁻¹, respectively. These interlayer modes require strong layer–layer coupling in WS₂/MoS₂, thus indicating that the interface between the monolayers is clean.³⁷ Therefore, the full dry-transfer method we used can produce a clean heterostructure interface.

To further characterize the heterostructure, we measured the PL spectrum at room temperature with 2.54 eV excitation energy and 3 × 10² W/cm² input power. Figure 2a shows the PL spectrum, where PL emissions from intralayer excitons in the WS₂ and MoS₂ samples can be seen at 2.00 and 1.88 eV, respectively.^{7,12,33} In addition, the heterostructure produces additional PL peaks at energies significantly lower than those of intralayer excitons, which are in the range of 1.3–1.7 eV. These additional peaks occur only in heterostructure samples,^{12,29} and we hypothesize that these peaks correspond to emissions from interlayer excitons. Peak decomposition analysis of the additional peaks (Figure 2b) has revealed the existence of three peaks at 1.63, 1.52, and 1.44 eV, which are respectively referred to as I₁, I₂, and I₃ in the following discussion. We prepared several heterostructure samples with a stacking angle of ~60° as discussed above, and the interlayer exciton peaks appear in the PL spectra in all cases (Figures S3 and S4); peak positions of I₁–I₃ slightly change depending on samples, and statistics on the peak positions are shown in Figure S4. We also prepared heterostructure samples with stacking angles from 0 to 30°. In these samples, the peak positions and appearance of I₁–I₃ depend on the stacking angle (Figure S5). These results

are consistent with the hypothesis that these peaks originate from interlayer excitons.^{12,13,27} Note that the I₁–I₃ peaks merge into a single broad peak in previously reported PL spectra of WS₂/MoS₂ probably due to inhomogeneous broadening caused by the substrate.¹² This achievement over previous results clearly demonstrates that the hBN encapsulation structure used in this study suppresses inhomogeneous broadening to obtain sufficiently fine-grain spectra data from the heterostructure itself.

To exclude the possibility that I₁–I₃ originate from bound excitons trapped at impurities or defect sites, we also measured exciton diffusion lengths through observations of PL images. The diffusion length of bound excitons should be nearly zero because bound excitons are localized around defects, while free excitons can diffuse over several hundred nanometers or even micrometers.^{38,39} Figure 3a,b shows a PL image of WS₂/MoS₂

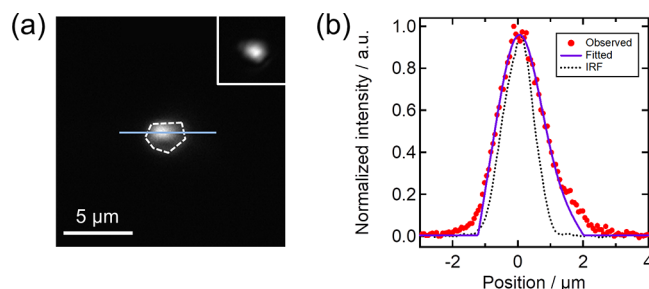


Figure 3. (a) Typical PL image of I₃ in hBN/WS₂/MoS₂/hBN excited by 2.43 eV light. White dotted line marks the edge of the sample. The inset shows the laser profile. (b) Cross-sectional profile of the PL image of hBN/WS₂/MoS₂/hBN and excitation laser (instrument response function, IRF).

and its corresponding cross-sectional profile, respectively. The PL image was taken with photon energy less than 1.51 eV (region of I₃) at room temperature. The inset of Figure 3a is an image of the laser beam used to excite the sample, and its corresponding cross-sectional profile is also shown in Figure 3b; excitation energy of 2.43 eV was used. It can be clearly observed that the PL image is broader than that of the corresponding excitation laser beam; this suggests that excitons created by the incident photons diffuse along the 2D plane. The PL image includes broadening arising not only from exciton diffusion but also from the laser spot size and the diffraction limit. Under the assumption that the broadening from the laser spot and the diffraction limit can be modeled as a Gaussian function, we have fitted the line profile of the PL image with the

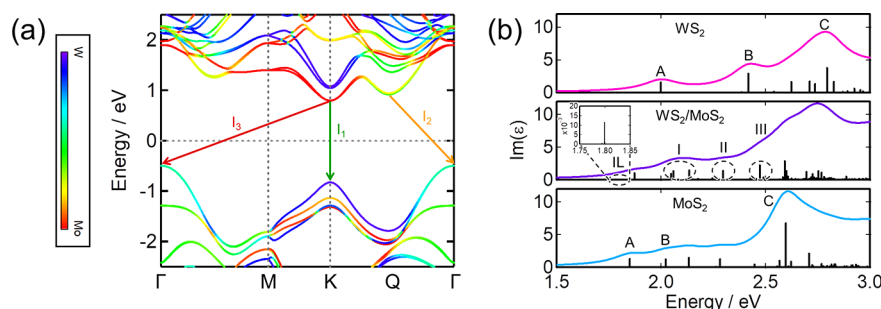


Figure 4. (a) DFT band structure of WS₂/MoS₂ heterostructure. Projections of bands onto individual layers are shown with a color gradient map. (b) Imaginary part of the dielectric function $\epsilon(\omega)$ obtained by solving the Bethe–Salpeter equation with G_0W_0 , depicting the optical absorption spectrum of WS₂/MoS₂ heterostructure (middle) along with the spectra from monolayer MoS₂ (top) and WS₂ (bottom). Vertical bars denote calculated oscillator strengths at the transition energy. The relative angle of 60° and the AA' stacking configuration are used in this calculation.

following diffusion equation (see Supporting Information for details):

$$\frac{\partial N}{\partial t} = D \left(\frac{\partial^2 N}{\partial x^2} + \frac{\partial^2 N}{\partial y^2} \right) - \frac{N}{\tau}$$

where N , D , x , y , t , and τ correspond to the number of excitons, diffusion coefficient, x coordinate, y coordinate, time, and lifetime of excitons, respectively. The differential equation can be solved numerically, yielding D values of 50, 15, and 30 cm²/s for I_1 , I_2 and I_3 , respectively (for details of the calculation, please see Figure S6). These large diffusion constants are obviously consistent with mobile excitons rather than localized excitons. In addition, we have measured excitation power dependence of intensities of I_1 – I_3 peaks to further exclude the possibility that the origin of I_1 – I_3 is bound excitons. As shown in Figure S7, intensities of I_1 – I_3 peaks show linear relations, where a constant α in $I_{\text{ex}} = c \times I_{\text{laser}}^\alpha$ (where I_{ex} is the intensity of interlayer exciton peak, c is a constant, I_{laser} is the intensity of the excitation laser) is 1.1, 0.91, and 0.97 for I_1 , I_2 , and I_3 , respectively. This linear relation is inconsistent to bound excitons because, in the case of bound excitons, α should be much smaller than 1 due to the intensity saturation caused by limited number of bound centers.

To address the origin of the I_1 – I_3 peaks in detail, we calculated the electronic band structure of WS₂/MoS₂ using density functional theory (DFT). We used a stacking angle of 60° in this calculation. As seen in the calculated band structure (shown in Figure 4a), the conduction band originates from MoS₂, whose CBM is located at the K valley, whereas the valence band originates from both MoS₂ and WS₂ with VBM located at the Γ valley. This structure implies that photoexcited carriers should form interlayer excitons in WS₂/MoS₂ after relaxation. Four valleys can contribute to optical transitions in this system, that is, the valleys located at the K and Γ points in the valence band and the valleys located at the K and Q points in the conduction band. The Q point is located between the K and Γ points in the Brillouin zone. One of the indicators for the origin of I_1 – I_3 is their spectral shape. Table 1 lists the full width at half-maximum (fwhm) and (Gaussian component)/(Lorentzian component) ratios of I_1 – I_3 obtained through peak fitting with the Voigt function. As shown in this table, the fwhm and the (Gaussian component)/(Lorentzian component) ratio of I_1 are much smaller than those of I_2 and I_3 . This strongly indicates that a broadening factor is involved in the I_2 and I_3 peaks, such as phonon emission and absorption. Considering

Table 1. Full Width at Half-Maximum and Ratio of Gaussian and Lorentzian Components of Interlayer Excitons Fitted with a Voigt Function

peak	fwhm/meV	ratio of Gaussian/Lorentzian fwhm
I_1	27	3.7×10^{-1}
I_2	123	2.8
I_3	69	6.3

the energies of the K, Γ , and Q valleys, we conclude that I_1 , I_2 , and I_3 indicate direct K–K interlayer excitons, indirect Q– Γ interlayer excitons, and indirect K– Γ interlayer excitons, respectively. Although the conclusion that three transitions (K–K, K– Γ , and Q– Γ) that should be the origin of the low-energy PL peaks does not depend on detailed stacking configuration and interlayer distance used in DFT calculations, it should be noted that strict assignment of the peaks is contingent on a very accurate estimate of interlayer distance in WS₂/MoS₂ in DFT calculations (please see Figure S8 and discussion therein). The temperature dependence of the peak positions of I_1 , I_2 , and I_3 is consistent with these assignments. As shown in Figure S3, the peak positions of I_1 – I_3 depend differently on temperature; this indicates that excitons corresponding to I_1 – I_3 originate from different valleys.

For further exploration of the origin of these excitonic peaks, we calculated the dielectric response $\epsilon(\omega)$ for both monolayers and the whole heterostructure. We solved the Bethe–Salpeter equation with G_0W_0 to correctly determine the quasiparticle energies and electron–hole interactions in these excitonic systems. The imaginary part of the dielectric function ϵ is directly related to the optical spectra of the material; thus, peaks in $\text{Im}(\epsilon)$ are reflected exactly in the absorption spectra. The optical spectra calculated for the monolayers (Figure 4b) show the A exciton peak to be at ~ 1.85 and ~ 2.0 eV for MoS₂ and WS₂, respectively, which matches very well with the observed peaks from intralayer excitons (Figure 2a). The calculated binding energies for the A exciton peak are ~ 0.55 and ~ 0.45 eV for MoS₂ and WS₂, respectively. In addition, the peak positions for the B and C excitons are in good agreement with those observed in previous studies.^{40,41} The calculated absorption spectrum of the heterostructure shown in Figure 4b is not simply a superposition of those of the two monolayers. The peak positions in the heterostructure are slightly shifted when compared with the positions observed from individual monolayers. The absorption spectrum for the heterostructure also includes a distinctive feature corresponding to interlayer

excitations. An interlayer excitonic peak can be observed in Figure 4b at 1.79–1.80 eV. This peak was also observed in a previous study on heterostructures.⁴¹ The calculated oscillator strength for this interlayer exciton peak is found to be 1.3% of the intralayer MoS₂ exciton peak, which is explained by noting that the electrons and holes are separated into two different monolayers, thus reducing the overlap of the electron and hole wave functions. We calculated a quasiparticle band gap of 2.06 eV for the heterostructure that corresponds to an exciton binding energy of 0.27 eV for the interlayer exciton, which is similar in magnitude to that of the intralayer excitons. In this calculation, only optical responses corresponding to vertical transitions are represented, and the appearance of a single peak in the calculated optical spectra of WS₂/MoS₂ is consistent with our conclusion that I₁ originates from direct excitons, whereas I₂ and I₃ arise from indirect excitons.

Figure 5 plots time-resolved PL intensities of interlayer excitons measured at room temperature. Fitting the exper-

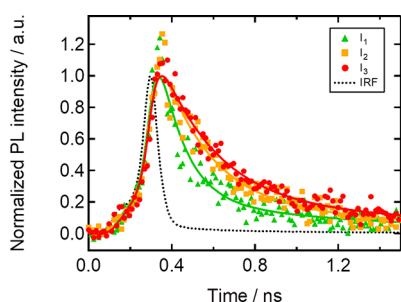


Figure 5. Time-resolved PL intensity of I₁, I₂, and I₃ of hBN/WS₂/MoS₂/hBN. Dashed line corresponds to the IRF.

imental data to a double exponential model yields relaxation times of the principal component of I₁ (τ_1), I₂ (τ_2), and I₃ (τ_3) of 116 ± 7 , 210 ± 13 , and 243 ± 12 ps, respectively. τ_2 and τ_3 are almost twice as long as τ_1 , and this is consistent with the peak assignment above; indirect interlayer excitons should have longer radiative decay lifetimes.²¹ The room-temperature lifetime obtained is on the order of several hundreds of picoseconds, which is shorter than the lifetime of interlayer excitons previously reported in other heterostructures at low temperatures, including MoSe₂/WSe₂.^{1,21,22} The PL lifetime of

interlayer excitons has been proven to depend strongly on temperature, where the lifetime is significantly shorter at high temperatures.^{21,22} Thus, the lifetime that we observed is consistent with previous results (additional data is shown in Figure S9).

The interlayer nature of this peak can be further confirmed by observing the dependence of emission intensity on excitation energy. Figure 6a shows a PLE intensity plot measured at 40 K with input power of 0.52–0.90 $\mu\text{J}/\text{cm}^2$. The PL spectra depend strongly on excitation energy. The region marked in red in Figure 6a plots the excitation energy dependence of emissions from a mixture of I₂ and I₃. In this spectral region, three peaks appear close to 2.08, 2.24, and 2.47 eV excitation energies, as seen in Figure 6b. In order to trace the origin of the peaks in the PLE spectrum of the heterostructure, we compared positions of the regions I, II, and III with peak positions in calculated absorption spectra for individual monolayers. It is clear that both layers, MoS₂ and WS₂, contribute individually to peaks in region I; namely, peaks in this region match with the WS₂ A exciton and MoS₂ B exciton. Region II matches with excitations in the MoS₂ layer, whereas region III is dominated by excitations from the WS₂ layer. Region I has greater intensity due to addition of excitations from both monolayers. This explains the large absorption cross section between 2.0 and 2.1 eV resulting in increased emission seen in Figure 6a. Due to type-II staggered band alignment and very rapid^{15,36} charge transfer in WS₂/MoS₂, interlayer excitons will form whenever individual monolayers are excited selectively, as electrons will transfer to MoS₂ when WS₂ is excited and holes will transfer to WS₂ when MoS₂ is excited. Therefore, interlayer excitons will appear and give distinct emissions in all three (I, II, and III) excitation regions. These considerations lead to the conclusion that the emission at 1.50–1.62 eV in Figure 6(b), with significant intensity in all three excitation regions, is an interlayer exciton peak. The emission around 1.73 eV (region of I₁) in Figure 6b shows a similar tendency with excitation photon energy but has lower intensity, most likely due to different excited carrier relaxation pathways. We also calculated the joint density of states (JDOS), which can provide insights into carrier relaxation pathways.⁴² Figure 6c shows the calculated JDOS. The JDOS corresponds to the band structure in Figure 4a. It

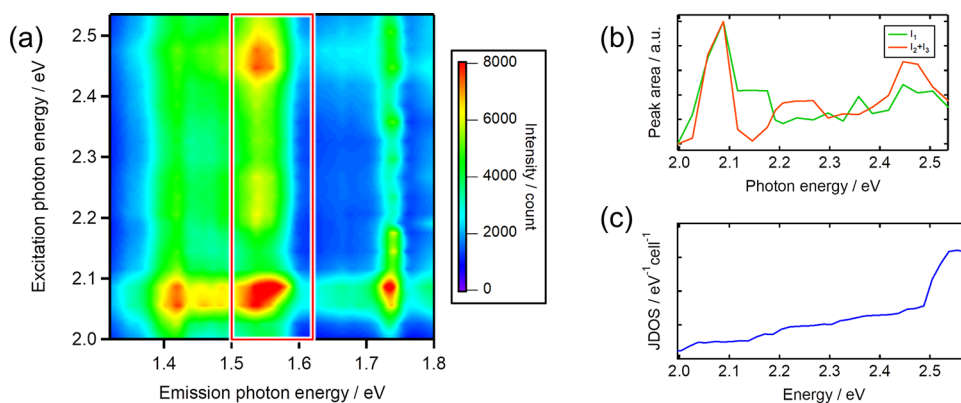


Figure 6. (a) Photoluminescence emission intensity plot for hBN/WS₂/MoS₂/hBN at 40 K with an excitation power of 0.52–0.90 $\mu\text{J}/\text{cm}^2$. Region where the intensity of PL is over 8000 counts is colored red. (b) Integrated PL intensity of the interlayer exciton peaks at 1.70–1.77 eV (region of I₁) and 1.50–1.62 eV (region of mixture of I₂ and I₃). (c) Joint density of states of WS₂/MoS₂ heterostructure obtained from DFT calculations. Some absorption peaks are due to excited states of excitons and thus cannot be captured by a single-particle description of ϵ_2 under random phase approximation.

has been shifted upward by 0.39 eV, to match the average difference between the MoS₂ and WS₂ band gaps at the K point and the positions of the intralayer MoS₂ and WS₂ PL peaks that appear at 1.94 and 2.07 eV, respectively (Figure S10).

The observed intensity of the PLE spectrum shown in Figure 6b has three peaks at 2.08, 2.24, and 2.47 eV, and only the peak at 2.47 eV matches the features in the JDOS plot; similar tendency can also be seen in Figure 6c. This result shows that excitonic effects play an important role in the response of the WS₂/MoS₂ heterostructure, and its absorption properties cannot be modeled appropriately with single-particle Kohn–Sham wavefunctions. The peak in JDOS is located in a band-nesting region, where the PL intensity from indirect excitons shows a pronounced peak. However, I₁ shows a less-pronounced peak in this energy region (Figure 6b), which suggests that indirect excitons are formed more efficiently than the direct excitons in this energy region. When a photo-excitation creates carriers in the band-nesting region, the created electrons and holes relax in opposite directions in *k*-space, and this may facilitate the formation of indirect excitons.⁴² This factor may explain the observed difference in the PLE spectra measured from indirect and direct excitons.

CONCLUSION

In summary, we have developed a fabrication method for hBN-encapsulated TMD-based heterostructures in which we can control the stacking angle. Our method is based on the full dry-transfer technique, which enables us to fabricate heterostructures with clean interfaces. The fabricated heterostructures, hBN/WS₂/MoS₂/hBN or WS₂/MoS₂/hBN, produce PL spectra that include PL peaks from intralayer and interlayer excitons. The PL peak from interlayer excitons can be decomposed into three peaks, and observing these peaks was possible because of the suppression of inhomogeneous broadening of PL spectra. Optical measurements and theoretical analyses revealed that these three PL peaks originate from direct K–K interlayer excitons, indirect Q–Γ interlayer excitons, and indirect K–Γ interlayer excitons. Our results suggest that vdW heterostructures composed of multivalley systems can host various interlayer excitons, which may have different exciton dispersions, decay lifetimes, and valley depolarization lifetimes. This is an important implication for the development of valleytronic devices with TMD-based vdW heterostructures.

METHODS

CVD Growth of WS₂ on Sapphire (*c*-Plane). We have grown monolayer WS₂ by the CVD method. We deposited tungsten (Nilaco, 99.95%) on a sapphire substrate, and elemental sulfur (Sigma-Aldrich, 99.98%) was supplied to the W-deposited substrate placed in a quartz tube. The inner diameter of quartz tube is 26 mm. Prior to the sulfurization reaction, W deposited on the substrate was oxidized at 700 °C under air flow. The quartz tube was heated with a three-zone furnace at 221, 400, and 900 °C for 60 min under an Ar flow of 400 sccm. The sulfur- and W-deposited substrates were placed at the coolest and hottest zones, respectively.

CVD Growth of MoS₂ on Exfoliated hBN. We have grown MoS₂ monolayers onto hBN by the CVD method. As precursors, elemental sulfur (Sigma-Aldrich, 99.98%) and molybdenum oxide (MoO₃, Sigma-Aldrich, 99.5%) were used. As a substrate for synthesizing MoS₂ monolayers, we prepared thin hBN flakes on a quartz substrate by the mechanical exfoliation method. Sulfur, MoO₃, and an hBN substrate were placed in a 26 mm inner diameter quartz tube. To avoid rapid sulfurization of MoO₃, the MoO₃ was placed in an inner quartz

tube with an inner diameter of 10 mm. The quartz tubes were heated with a three-zone furnace at 200, 750, and 1100 °C for 20 min under an Ar flow of 200 sccm; sulfur, MoO₃, and a substrate with hBN flakes were placed at the coolest, medium, and hottest zones, respectively.

Fabrication of hBN-Encapsulated Heterostructures. hBN flakes were prepared on 100 nm SiO₂/Si substrates by the mechanical exfoliation method. One of the hBN flakes on a SiO₂/Si was picked up by a PMMA (Microchem A11)/PDMS (Shin-Etsu Silicone KE-106) film on a glass slide, and then a monolayer WS₂ flake grown on a sapphire substrate was picked up with the hBN/PMMA/PDMS film. PMMA was used to improve the successful rate of the hBN pickup. The prepared stacked structure, WS₂/hBN/PMMA/PDMS, was then transferred onto a MoS₂/hBN on a quartz substrate to form a heterostructure, hBN/WS₂/MoS₂/hBN. To achieve sufficient interlayer contact, we heated the substrate during the transfer process, and the PMMA/PDMS film was detached from the prepared heterostructure by cooling the substrate. All the processes, pick-up and transfer process, were performed with a home-built manipulation system equipped with an optical microscope and stepping motor stages. After the fabrication of a heterostructure, we heated samples under vacuum at 200 °C over 10 h.

Photoluminescence and Raman Measurement. We obtained PL images by a fluorescence microscope (Leica TCS SP8 gSTED) at room temperature. To obtain the image, an excitation wavelength of 488 nm was used. Room-temperature PL and Raman spectra were measured by using a confocal Raman microscope (Renishaw InVia Raman and Horiba Jobin Yvon LabRAM HR-800) with 488 nm CW laser excitation (COHERENT Sapphire 488 LP). In PLE measurements and time-resolved PL measurements, we used a home-built microspectroscopy system equipped with a spectrometer (Princeton Instruments IsoPlane SCT320) and a supercontinuum laser system (NKT Photonics SuperK EXTREME); laser beam from the supercontinuum laser was monochromated by a spectrometer (Princeton Instruments SP2150). In low-temperature measurements, we placed a sample in a cryostat (CryoVac KONTI-Cryostat-Micro) with continuous flowing of liquid He or N₂ under a vacuum of ~10⁻⁴ Pa; CryoVac TIC 304-MA was used to control temperature. Objective lenses (50–100× and 0.7–0.85 NA) were used for all measurements.

First-Principles Calculations. First-principles DFT calculations were performed using the Vienna Ab Initio Simulation Package.⁴³ Ion–electron interactions were represented by all-electron projector-augmented wave potentials.⁴⁴ The generalized gradient approximation parametrized by Perdew–Burke–Ernzerhof⁴⁵ was used to account for the electronic exchange and correlation. The wave functions were expanded in a plane wave basis with energy cutoff of 500 eV. The structure was relaxed until the components of Hellmann–Feynman forces on the atoms were less than 10⁻⁴ eV/Å, and an optimized lattice constant of 3.18 Å was obtained for both MoS₂ and WS₂. The heterostructure was constructed from the primitive cells of MoS₂ and WS₂ with the stacking similar to that found in 2H-MoS₂. A vacuum of 20 Å was used in all the calculations. The interlayer spacing in the heterostructure was optimized using the optB86b-vdW⁴⁶ functional to approximately account for dispersion interactions, and a value of 6.24 Å was obtained. Spin–orbit coupling was included in all the calculations. Optical spectra were calculated using single-shot G₀W₀ procedure together with solution of the Bethe–Salpeter equation in the Tamm–Dancoff approximation.^{47,48} This technique correctly accounts for electron–hole interaction necessary to obtain an accurate excitonic spectra. Γ-centered grids of 18 × 18 × 1 and 15 × 15 × 1 were used to sample the Brillouin zone for monolayers and heterostructures, respectively. A total of 182 bands, which includes 156 empty bands, was used for monolayers, whereas 280 bands with 224 empty bands were included for the heterostructure. These parameters were optimized to obtain a converged optical spectrum.

ASSOCIATED CONTENT

Supporting Information

The Supporting Information is available free of charge on the ACS Publications website at DOI: 10.1021/acsnano.7b08253.

Characterization of CVD-grown monolayer WS₂ and MoS₂, low-frequency Raman spectrum of hBN/WS₂/MoS₂/hBN, characterization of CVD-grown WS₂/MoS₂/hBN, statistics on the peak position of the low-energy PL peaks, PL spectra of hBN/WS₂/MoS₂/hBN with different stacking angle, details on the determination of the diffusion constant, excitation power dependence of the low-energy PL peaks, DFT calculation of transition energies of WS₂/MoS₂, another example of time-resolved PL intensity of hBN/WS₂/MoS₂/hBN, and a PL spectrum from intralayer excitons at low temperature (PDF)

AUTHOR INFORMATION

Corresponding Authors

*E-mail: noris@nagoya-u.jp.

*E-mail: r.kitaura@nagoya-u.jp.

ORCID

Alex Kutana: 0000-0001-6405-6466

Hisanori Shinohara: 0000-0001-9400-7622

Ryo Kitaura: 0000-0001-8108-109X

Author Contributions

[†]M.O. and A.K. contributed equally to this work.

Notes

The authors declare no competing financial interest.

ACKNOWLEDGMENTS

This work was supported by JSPS KAKENHI Grant Nos. JP16H06331, JP16H03825, JP16H00963, JP15K13283, and JP25107002. This work is also supported by World Premier International Research Center, Advanced Institute for Materials Research and the Global COE Program in Chemistry, Nagoya University. M.O. thanks the Research Fellowship for Young Scientists supported by JSPS. Work at Rice by A.K., S.G., and B.I.Y. (theoretical/computational analysis) was supported by the Army Research Office Grant W911NF-16-1-0255. We thank K. Itami and Y. Miyauchi for sharing the Raman apparatus. We are grateful to T. Higashiyama and Y. Sato for letting us use the fluorescence microscope. We thank T. Machida and S. Masubuchi for their advice on mechanical exfoliation. We also thank K. Nagashio and T. Uwanno for their fruitful discussion and advice on the fabrication of heterostructures. We are also grateful to K. Matsuda, Y. Miyauchi, and Y. Hasegawa for help in optical measurement and their advice.

REFERENCES

- (1) Rivera, P.; Schaibley, J. R.; Jones, A. M.; Ross, J. S.; Wu, S.; Aivazian, G.; Klement, P.; Seyler, K.; Clark, G.; Ghimire, N. J.; Yan, J.; Mandrus, D. G.; Yao, W.; Xu, X. Observation of Long-Lived Interlayer Excitons in Monolayer MoSe₂-WSe₂ Heterostructures. *Nat. Commun.* **2015**, *6*, 6242.
- (2) Rivera, P.; Seyler, K. L.; Yu, H.; Schaibley, J. R.; Yan, J.; Mandrus, D. G.; Yao, W.; Xu, X. Valley-Polarized Exciton Dynamics in a 2D Semiconductor Heterostructure. *Science* **2016**, *351*, 688–691.
- (3) Kim, J.; Jin, C.; Chen, B.; Cai, H.; Zhao, T.; Lee, P.; Kahn, S.; Watanabe, K.; Taniguchi, T.; Tongay, S.; Crommie, M. F.; Wang, F. Observation of Ultralong Valley Lifetime in WSe₂/MoS₂ Heterostructures. *Sci. Adv.* **2017**, *3*, e1700518.
- (4) Furchi, M. M.; Pospischil, A.; Libisch, F.; Burgdörfer, J.; Mueller, T. Photovoltaic Effect in an Electrically Tunable van der Waals Heterojunction. *Nano Lett.* **2014**, *14*, 4785–4791.

- (5) Yan, X.; Liu, C.; Li, C.; Bao, W.; Ding, S.; Zhang, D. W.; Zhou, P. Tunable SnSe₂/WSe₂ Heterostructure Tunneling Field Effect Transistor. *Small* **2017**, *13*, 1701478.

- (6) Lee, C.; Yan, H.; Brus, L. E.; Heinz, T. F.; Hone, J.; Ryu, S. Anomalous Lattice Vibrations of Single- and Few-layer MoS₂. *ACS Nano* **2010**, *4*, 2695–2700.

- (7) Mak, K. F.; Lee, C.; Hone, J.; Shan, J.; Heinz, T. F. Atomically Thin MoS₂: a New Direct-Gap Semiconductor. *Phys. Rev. Lett.* **2010**, *105*, 136805.

- (8) Xiao, D.; Liu, G.-B.; Feng, W.; Xu, X.; Yao, W. Coupled Spin and Valley Physics in Monolayers of MoS₂ and Other Group-VI Dichalcogenides. *Phys. Rev. Lett.* **2012**, *108*, 196802.

- (9) Eda, G.; Yamaguchi, H.; Voiry, D.; Fujita, T.; Chen, M.; Chhowalla, M. Photoluminescence from Chemically Exfoliated MoS₂. *Nano Lett.* **2011**, *11*, 5111–5116.

- (10) Wurstbauer, U.; Miller, B.; Parzinger, E.; Holleitner, A. W. Light–Matter Interaction in Transition Metal Dichalcogenides and Their Heterostructures. *J. Phys. D: Appl. Phys.* **2017**, *50*, 173001.

- (11) Uwanno, T.; Hattori, Y.; Taniguchi, T.; Watanabe, K.; Nagashio, K. Fully Dry PMMA Transfer of Graphene on h-BN Using a Heating/Cooling System. *2D Mater.* **2015**, *2*, 041002.

- (12) Gong, Y.; Lin, J.; Wang, X.; Shi, G.; Lei, S.; Lin, Z.; Zou, X.; Ye, G.; Vajtai, R.; Yakobson, B. I.; Terrones, H.; Terrones, M.; Tay, B. K.; Lou, J.; Pantelides, S. T.; Liu, Z.; Zhou, W.; Ajayan, M. P. Vertical and In-Plane Heterostructures from WS₂/MoS₂ Monolayers. *Nat. Mater.* **2014**, *13*, 1135–1142.

- (13) Tongay, S.; Fan, W.; Kang, J.; Park, J.; Koldemir, U.; Suh, J.; Narang, D. S.; Liu, K.; Ji, J.; Li, J.; Sinclair, R.; Wu, J. Tuning Interlayer Coupling in Large-Area Heterostructures with CVD-Grown MoS₂ and WS₂ Monolayers. *Nano Lett.* **2014**, *14*, 3185–3190.

- (14) Zhang, J.; Wang, J.; Chen, P.; Sun, Y.; Wu, S.; Jia, Z.; Lu, X.; Yu, H.; Chen, W.; Zhu, J.; Xie, G.; Yang, R.; Shi, D.; Xu, X.; Xiang, J.; Liu, K.; Zhang, G. Observation of Strong Interlayer Coupling in MoS₂/WS₂ Heterostructures. *Adv. Mater.* **2016**, *28*, 1950–1956.

- (15) Chen, H.; Wen, X.; Zhang, J.; Wu, T.; Gong, Y.; Zhang, X.; Yuan, J.; Yi, C.; Lou, J.; Ajayan, P. M.; Zhuang, W.; Zhang, G.; Zheng, J. Ultrafast Formation of Interlayer Hot Excitons in Atomically Thin MoS₂/WS₂ Heterostructures. *Nat. Commun.* **2016**, *7*, 12512.

- (16) Ding, Y.; Wang, Y.; Ni, J.; Shi, L.; Shi, S.; Tang, W. First Principles Study of Structural, Vibrational and Electronic Properties of Graphene-Like MX₂ (M= Mo, Nb, W, Ta; X= S, Se, Te) Monolayers. *Phys. B* **2011**, *406*, 2254–2260.

- (17) Mak, K. F.; He, K.; Shan, J.; Heinz, T. F. Control of Valley Polarization in Monolayer MoS₂ by Optical Helicity. *Nat. Nanotechnol.* **2012**, *7*, 494–498.

- (18) Kumar, A.; Ahluwalia, P. K. Electronic Structure of Transition Metal Dichalcogenides Monolayers 1H-MX₂ (M= Mo, W; X= S, Se, Te) from *ab-initio* Theory: New Direct Band Gap Semiconductors. *Eur. Phys. J. B* **2012**, *85*, 186.

- (19) Xu, X.; Yao, W.; Xiao, D.; Heinz, T. F. Spin and Pseudospins in Layered Transition Metal Dichalcogenides. *Nat. Phys.* **2014**, *10*, 343–350.

- (20) Wang, G.; Bouet, L.; Lagarde, D.; Vidal, M.; Balocchi, A.; Amand, T.; Marie, X.; Urbaszek, B. Valley Dynamics Probed Through Charged and Neutral Exciton Emission in Monolayer WSe₂. *Phys. Rev. B: Condens. Matter Mater. Phys.* **2014**, *90*, 075413.

- (21) Miller, B.; Steinhoff, A.; Pano, B.; Klein, J.; Jahnke, F.; Holleitner, A.; Wurstbauer, U. Long-Lived Direct and Indirect Interlayer Excitons in van der Waals Heterostructures. *Nano Lett.* **2017**, *17*, 5229–5237.

- (22) Nagler, P.; Plechinger, G.; Ballottin, M. V.; Mitioglu, A.; Meier, S.; Paradiso, N.; Strunk, C.; Chernikov, A.; Christianen, P. C. M.; Schüller, C.; Korn, T. Interlayer Exciton Dynamics in a Dichalcogenide Monolayer Heterostructure. *2D Mater.* **2017**, *4*, 025112.

- (23) Godde, T.; Schmidt, D.; Schmutzler, J.; Aßmann, M.; Debus, J.; Withers, F.; Alexeev, E. M.; Del Pozo-Zamudio, O.; Skrypkina, O. V.; Novoselov, K. S.; Bayer, M.; Tartakovskii, A. I. Exciton and Trion Dynamics in Atomically Thin MoSe₂ and WSe₂: Effect of Localization. *Phys. Rev. B: Condens. Matter Mater. Phys.* **2016**, *94*, 165301.

- (24) Zhu, C. R.; Zhang, K.; Glazov, M.; Urbaszek, B.; Amand, T.; Ji, Z. W.; Liu, B. L.; Marie, X. Exciton Valley Dynamics Probed by Kerr Rotation in WSe₂ Monolayers. *Phys. Rev. B: Condens. Matter Mater. Phys.* **2014**, *90*, 161302.
- (25) Komsa, H.-P.; Krashennnikov, A. V. Electronic Structures and Optical Properties of Realistic Transition Metal Dichalcogenide Heterostructures from First Principles. *Phys. Rev. B: Condens. Matter Mater. Phys.* **2013**, *88*, 085318.
- (26) Heo, H.; Sung, J. H.; Cha, S.; Jang, B.-G.; Kim, J.-Y.; Jin, G.; Lee, D.; Ahn, J.-H.; Lee, M.-J.; Shim, J. H.; Choi, H.; Jo, M.-H. Interlayer Orientation-Dependent Light Absorption and Emission in Monolayer Semiconductor Stacks. *Nat. Commun.* **2015**, *6*, 7372.
- (27) Yu, H.; Wang, Y.; Tong, Q.; Xu, X.; Yao, W. Anomalous Light Cones and Valley Optical Selection Rules of Interlayer Excitons in Twisted Heterobilayers. *Phys. Rev. Lett.* **2015**, *115*, 187002.
- (28) Nayak, P. K.; Horbatenko, Y.; Ahn, S.; Kim, G.; Lee, J.-U.; Ma, K. Y.; Jang, A.-R.; Lim, H.; Kim, D.; Ryu, S.; Cheong, H.; Park, N.; Shin, H. S. Probing Evolution of Twist-Angle-Dependent Interlayer Excitons in MoSe₂/WSe₂ van der Waals Heterostructures. *ACS Nano* **2017**, *11*, 4041–4050.
- (29) Kobayashi, Y.; Yoshida, S.; Sakurada, R.; Takashima, K.; Yamamoto, T.; Saito, T.; Konabe, S.; Taniguchi, T.; Watanabe, K.; Maniwa, Y.; Takeuchi, O.; Shigekawa, H.; Miyata, Y. Modulation of Electrical Potential and Conductivity in an Atomic-Layer Semiconductor Heterojunction. *Sci. Rep.* **2016**, *6*, 31223.
- (30) Hill, H. M.; Rigosi, A. F.; Rim, K. T.; Flynn, G. W.; Heinz, T. F. Band Alignment in MoS₂/WS₂ Transition Metal Dichalcogenide Heterostructures Probed by Scanning Tunneling Microscopy and Spectroscopy. *Nano Lett.* **2016**, *16*, 4831–4837.
- (31) Okada, M.; Sawazaki, T.; Watanabe, K.; Taniguchi, T.; Hibino, H.; Shinohara, H.; Kitaura, R. Direct Chemical Vapor Deposition Growth of WS₂ Atomic Layers on Hexagonal Boron Nitride. *ACS Nano* **2014**, *8*, 8273–8277.
- (32) Yan, A.; Velasco, J.; Kahn, S.; Watanabe, K.; Taniguchi, T.; Wang, F.; Crommie, M. F.; Zettl, A. Direct Growth of Single- and Few-Layer MoS₂ on h-BN with Preferred Relative Rotation Angles. *Nano Lett.* **2015**, *15*, 6324–6331.
- (33) Gutiérrez, H. R.; Perea-López, N.; Elías, A. L.; Berkdemir, A.; Wang, B.; Lv, R.; López-Urías, F.; Crespi, V. H.; Terrones, H.; Terrones, M. Extraordinary Room-Temperature Photoluminescence in Triangular WS₂ Monolayers. *Nano Lett.* **2013**, *13*, 3447–3454.
- (34) van der Zande, A. M.; Huang, P. Y.; Chenet, D. A.; Berkelbach, T. C.; You, Y.; Lee, G.-H.; Heinz, T. F.; Reichman, D. R.; Muller, D. A.; Hone, J. C. Grains and Grain Boundaries in Highly Crystalline Monolayer Molybdenum Disulphide. *Nat. Mater.* **2013**, *12*, 554–561.
- (35) Mouri, S.; Zhang, W.; Kozawa, D.; Miyauchi, Y.; Eda, G.; Matsuda, K. Thermal Dissociation of Inter-Layer Excitons in MoS₂/MoSe₂ Hetero-Bilayers. *Nanoscale* **2017**, *9*, 6674–6679.
- (36) Hong, X.; Kim, J.; Shi, S.-F.; Zhang, Y.; Jin, C.; Sun, Y.; Tongay, S.; Wu, J.; Zhang, Y.; Wang, F. Ultrafast Charge Transfer in Atomically thin MoS₂/WS₂ Heterostructures. *Nat. Nanotechnol.* **2014**, *9*, 682–686.
- (37) Lui, C. H.; Ye, Z.; Ji, C.; Chiu, K.-C.; Chou, C.-T.; Andersen, T. I.; Means-Shively, C.; Anderson, H.; Wu, J.-M.; Kidd, T.; Lee, Y.-H.; He, R. Observation of Interlayer Phonon Modes in van der Waals Heterostructures. *Phys. Rev. B: Condens. Matter Mater. Phys.* **2015**, *91*, 165403.
- (38) Mouri, S.; Miyauchi, Y.; Toh, M.; Zhao, W.; Eda, G.; Matsuda, K. Nonlinear Photoluminescence in Atomically Thin Layered WSe₂ Arising from Diffusion-Assisted Exciton-Exciton Annihilation. *Phys. Rev. B: Condens. Matter Mater. Phys.* **2014**, *90*, 155449.
- (39) Kumar, N.; Cui, Q.; Ceballos, F.; He, D.; Wang, Y.; Zhao, H. Exciton Diffusion in Monolayer and Bulk MoSe₂. *Nanoscale* **2014**, *6*, 4915–4919.
- (40) Qiu, D. Y.; da Jornada, F. H.; Louie, S. G. Optical Spectrum of MoS₂: Many-Body Effects and Diversity of Exciton States. *Phys. Rev. Lett.* **2013**, *111*, 216805.
- (41) Palummo, M.; Bernardi, M.; Grossman, J. C. Exciton Radiative Lifetimes in Two-Dimensional Transition Metal Dichalcogenides. *Nano Lett.* **2015**, *15*, 2794–2800.
- (42) Kozawa, D.; Kumar, R.; Carvalho, A.; Kumar Amara, K.; Zhao, W.; Wang, S.; Toh, M.; Ribeiro, R. M.; Castro Neto, A. H.; Matsuda, K.; Eda, G. Photocarrier Relaxation Pathway in Two-Dimensional Semiconducting Transition Metal Dichalcogenides. *Nat. Commun.* **2014**, *5*, 4543.
- (43) Kresse, G.; Furthmüller, J. Efficiency of *ab-initio* Total Energy Calculations for Metals and Semiconductors Using a Plane-Wave Basis Set. *Comput. Mater. Sci.* **1996**, *6*, 15–50.
- (44) Blöchl, P. E. Projector Augmented-Wave Method. *Phys. Rev. B: Condens. Matter Mater. Phys.* **1994**, *50*, 17953–17979.
- (45) Perdew, J. P.; Burke, K.; Ernzerhof, M. Generalized Gradient Approximation Made Simple. *Phys. Rev. Lett.* **1996**, *77*, 3865–3868.
- (46) Klimeš, J.; Bowler, D. R.; Michaelides, A. Chemical Accuracy for the van der Waals Density Functional. *J. Phys.: Condens. Matter* **2010**, *22*, 022201.
- (47) Albrecht, S.; Reining, L.; Del Sole, R.; Onida, G. *Ab initio* Calculation of Excitonic Effects in the Optical Spectra of Semiconductors. *Phys. Rev. Lett.* **1998**, *80*, 4510–4513.
- (48) Rohlfing, M.; Louie, S. G. Electron-Hole Excitations in Semiconductors and Insulators. *Phys. Rev. Lett.* **1998**, *81*, 2312–2315.